# Superresolution of Coherent Sources in Real-Beam Data

**In this work we study the unique problems associated with resolving the direction of arrival (DOA) of coherent signals separated by less than an antenna beamwidth when the data are collected in the beamspace domain with, for example, electronically or holographically scanned antennas. We also propose a technique that is able to resolve these coherent signals. The technique is based on interpolation of the data measured by an element-space virtual array. Although the data are collected in the beamspace domain, the coherence structure can be broken by interpolating multiple shifted element-space virtual arrays. The efficacy of this technique depends on a fundamental tradeoff that arises due to a nonuniform signal-to-noise ratio (SNR) profile across the elements of the virtual array. This profile is due to the structure imposed by the specific beam pattern of the antenna. In addition to describing our technique and studying the SNR profile tradeoff, we also incorporate a strategy for improving performance through a subswath technique that improves covergence of covariance estimates.**

## I. INTRODUCTION

Superresolution of signals separated by less than an antenna beamwidth has received considerable attention in the array signal processing literature. Two common subspace-based superresolution techniques are MUSIC [1–4] and ESPRIT [5]. MUSIC works by decomposing the covariance matrix into a signal-plus-noise subspace and an orthogonal noise-only subspace using eigenvalue decomposition. The angles of arrival are estimated by projecting the array manifold onto the noise subspace. The inverse of the power spectrum of such a projection gives signal peaks in the estimated directions. ESPRIT [5] works by exploiting rotational invariance of the underlying signal subspace induced by requiring that the sensor array have translation invariance. Most of these methods, however, have been applied almost exclusively to multi-channel arrays. For example, techniques such as spatial smoothing [6], which enable resolution of coherent signals, can only be applied to antenna arrays that can be decomposed into multiple subarrays with identical structure except for a translational shift. If such a subarray structure is not available, then the subarray data can also be interpolated [7], but the underlying data collection domain is still in element space. Work has also been reported toward efficient implementation of techniques such as MUSIC. Of these techniques, root-MUSIC deserves special mention [2, 3].

There has, however, been little work reported on resolving signals within the antenna beamwidth when the sensor, instead of being a multi-channel array, collects data by scanning a real antenna beam over the possible directions of arrival (DOAs). Data collection in beamspace can occur using electronically and holographically scanned antennas having fast scanning capability but only a single output data channel. Consider a real-beam system that collects observations over an angular range of $\theta_-$ to $\theta_+$ with $N$ angular beam positions. The system has only one receiving channel. If the system has an antenna array, the single data output implies that the element signals are combined prior to downconversion and analog-to-digital conversion. On the other hand, a traditional antenna array used for direction finding will usually require separate analog-to-digital data streams for each antenna element, or at least from several subarrays.

Recently, Ly et al. [8] developed a scan-MUSIC (SMUSIC) algorithm for achieving angular superresolution with a single, stepped-frequency radar having a scanned, narrow-beam antenna. Their observed data are in matrix form with beam positions along columns and frequency steps along the rows. Once the matrix is obtained, each column is linearly averaged over all frequencies. This averaging results in a single vector, each element of which is a frequency-averaged observation from a particular angular direction. Ly et al. then go on to divide this beamspace vector into subvectors and apply subvector averaging as a form of spatial smoothing. The goal is to generate a covariance matrix of sufficient rank that it can be used to perform beamspace MUSIC. There is, however, a difficulty with this approach related to the covariance matrices for each subvector.[1] Different subvectors in beamspace correspond to measurements collected over different angular sectors. Since a given angle of arrival is not in the same relative position for all beam positions, a given signal's power profile is different in each subvector. (See Section IVD for more details.) As a result, averaging the covariance matrices of each of these subvectors results in poor performance because the source seems to be in a different location for each subvector.

Manuscript received June 17, 2008; revised February 5, 2009; released for publication May 9, 2009.

IEEE Log No. T-AES/46/3/937992.

Refereeing of this contribution was handled by S. D. Blunt.



[1] A data snapshot vector collected in beamspace corresponds to the entire angular range of interest as illustrated in Fig. 2(a). A subvector of the data snapshot vector corresponds to measurements taken over a certain portion of the entire angular range.

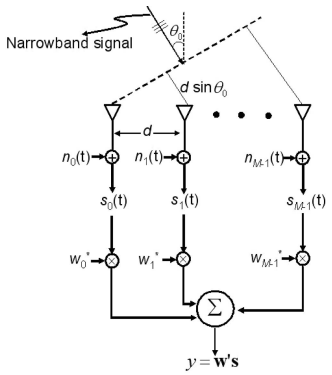


Fig. 1. Beamforming using the common electronically scanned phased array. Spatial frequency response is controlled by complex weight vector $\mathbf{w}$. The noise vector $\mathbf{n} = [n_0, n_1, \ldots, n_{M-1}]$, where $M$ is the number of sensors, corresponds to the AWGN case.

In this paper we propose a new technique for resolving coherent signals in data collected by a real-beam antenna. In Section II we introduce the data model. Section III briefly discusses coherent and noncoherent signals. In Section IV we introduce our proposed solution along with a discussion of the unique problems associated with covariance-based techniques when applied to real-beam superresolution of coherent signals. Our simulated results are given in Section V, and we conclude in Section VI.

## II. DATA MODEL

In the case of traditional uniform linear arrays (ULAs), data are collected in the element-space domain by spatially sampling the incoming signal. As shown in Fig. 1, the spatial sampling is performed by $M$ antenna elements whose multi-channel output $\mathbf{s} = [s_0(t), s_1(t), \ldots, s_{M-1}(t)]$ is sampled and then weighted by a complex weight vector $\mathbf{w}$. The complex weight vector emphasizes signals from a particular DOA while supressing others, thus performing beamforming [9, 10]. By changing the weight vector, the array beam can be electronically scanned to focus on a different DOA. The shape (linear, planar) and size (aperture size) of the array geometry and the number of sensors affect system performance by establishing basic system constraints.

In contrast, a real-beam antenna system collects data in the beamspace (spatial frequency or wavenumber) domain, and data collection is performed by sweeping a narrow beam through the entire field of view (FOV). The antenna beam stops to collect a measurement at each of several positions that are uniformly spaced in angle. Therefore, at each beam position, the contributions from all sources are weighted by the real-beam antenna pattern before being summed into a single output. The contribution due to a signal arriving from a particular DOA rises and falls as the mainlobe and sidelobes of the real beam's antenna pattern sweep across the FOV. A single sweep of the FOV results in a single data snapshot vector. We assume the signals to be narrowband.

Let $\theta$ be the source signal DOA and let $\gamma_i$ be the pointing angle of the $i$th beam position in azimuth. We first define $\mathbf{a}(\theta) = [a(\gamma_1, \theta), a(\gamma_2, \theta), \ldots, a(\gamma_{N_b}, \theta)]^{\mathrm{T}}$ to be the beamspace steering vector for a signal arriving from direction $\theta$ where $a(\gamma_i, \theta)$ is the response of the antenna due to the signal arriving from $\theta$ when steered to angle $\gamma_i$. Let the $\gamma_i$, $i = 1, 2, \ldots, N_b$ be the beam sweep positions (angles). We can now define the antenna response matrix (or beamspace manifold) as

$$\mathbf{A} = [\mathbf{a}(\theta_1), \mathbf{a}(\theta_2), \ldots, \mathbf{a}(\theta_{N_a})]$$

where $\theta_j$, $j = 1, 2, \ldots, N_a$ are the signal DOAs. Let $\mathbf{s}(k)$ be the $N_a \times 1$ vector of signal amplitudes during the $k$th sweep. Defining $s_j(k)$ as the signal amplitude due to the $j$th DOA during the $k$th sweep, the signal amplitude vector for the $k$th sweep is

$$\mathbf{s}(k) = [s_1(k), s_2(k), \ldots, s_{N_a}(k)]^{\mathrm{T}}. \tag{1}$$

We also define $\tilde{\mathbf{n}}(k)$ as the $N_b \times 1$ additive noise vector for a single sweep. The signal model is then given by

$$\tilde{\mathbf{y}}(k) = \mathbf{A}\mathbf{s}(k) + \tilde{\mathbf{n}}(k), \qquad k = 1, 2, \ldots, K \tag{2}$$

and the data vector $\tilde{\mathbf{y}}(k)$ for a single value of $k$ is a single beamspace data snapshot.

It is important to note that although (2) resembles a typical snapshot model for a multi-channel system, the elements of $\mathbf{A}$ have varying amplitude. The variation in amplitude is due to the real beam's directional gain, which results in unequal and varying weighting of the DOAs as the beam is scanned across the FOV.

## III. COHERENT AND NONCOHERENT SIGNALS

Given the snapshots $\tilde{\mathbf{y}}(k)$, $k = 1, 2, \ldots, K$, we define the data covariance matrix as $\mathbf{R}_{\tilde{\mathbf{y}}} = \mathrm{E}[\tilde{\mathbf{y}}\tilde{\mathbf{y}}^{\mathrm{H}}]$. The additive noise is assumed to be complex white Gaussian noise with variance $\sigma^2$. Using (2) and making the typical assumption of independence between the signal sources and the receiver noise, we get $\mathbf{R}_{\tilde{\mathbf{y}}} = \mathbf{A}\mathbf{R}_{\mathbf{s}}\mathbf{A}^{\mathrm{H}} + \sigma^2\mathbf{I}$, where $\mathbf{R}_{\mathbf{s}} = \mathrm{E}[\mathbf{s}\mathbf{s}^{\mathrm{H}}]$ is the signal covariance matrix. The white noise assumption is valid because, firstly, the different beam positions are scanned in time and, therefore, the receiver noise at one beam position is independent of the receiver noise at a different beam position. Secondly, the noise is due to the receiver, and as shown in (2), the antenna pattern has no effect on it.

If the signals are not coherent, then $\mathrm{rank}(\mathbf{R}_{\mathbf{s}}) = N_a$ (full rank), and we can apply any superresolution technique (e.g. MUSIC) directly in the beamspace domain as long as the beamspace manifold, or the physical beampattern, is accurately characterized. On the other hand, if the signals are coherent

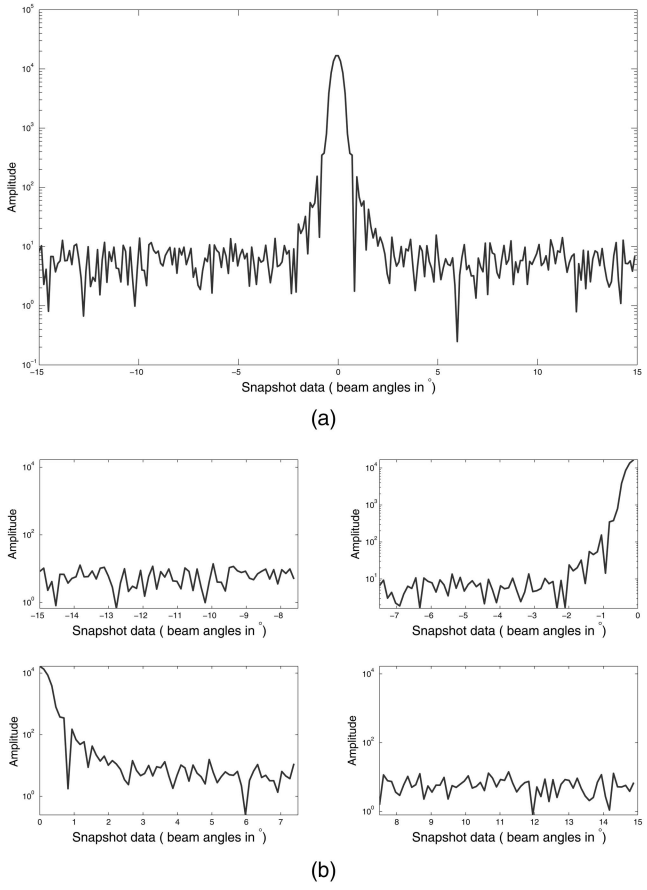


Fig. 2. (a) Data snapshot for a source arriving from 0°. (b) Subvectors (no overlap for conceptual convenience) generated from the data snapshot in (a). It can be seen that subvectors do not have identical structure because signal strength is function of angle. As a consequence, corresponding covariance matrices also will not have identical structure.

then rank($\mathbf{R_s}$) $\neq N_a$ and we cannot directly apply any superresolution technique. Coherent signals are defined as having perfectly correlated signal amplitudes that differ only by a constant. Therefore, they always add together in the same proportion, leading to a degenerate covariance matrix. Subspace-based superresolution techniques, unlike maximum likelihood (ML) methods,[2] achieve their performance by exploiting the structure of the data covariance matrix, which is ruined by a degenerate covariance matrix. To resolve such signals, their coherence must be broken. Canh Ly et al. [8] do this by employing smoothing in the beamspace domain. However, as mentioned in the Introduction, the angular range or sub-FOV of each subvector is different. Fig. 2(a) shows the beamspace data vector for a signal coming from 0°. On dividing this beamspace snapshot into subvectors as seen in Fig. 2(b), we see that the signal has a different power profile in different angular ranges. This causes the covariance matrices corresponding to the different subvectors to be unequal, which leads to degraded performance. To overcome this difficulty, we propose to interpolate the element-space data of several virtual antenna arrays [7], which can then be used in a spatial smoothing algorithm. Unfortunately, there are also problems associated with this method that arise from the structure associated with the beam pattern. We explain these problems in the next section where we also discuss our proposed solution.

[2]ML methods consider DOA estimation as a parameter estimation problem and often involve solving a multivariate maximization problem using numerical search methods [11, 12].

## IV. PROPOSED SOLUTION

Our proposed solution uses minimum-variance beamforming [9], though the MUSIC algorithm is also a reasonable alternative. Minimum-variance is a quadratic technique while MUSIC is a subspace method. The difference is that the minimum-variance technique considers the whole of signal space (the data covariance matrix, as is shown below) while MUSIC uses the noise subspace. As a result, minimum variance does not require the explicit step of separating the signal and noise subspaces as required in MUSIC. On the other hand, both approaches require the number of sources when using root-based techniques. Below, we describe our minimum-variance beamforming solution and discuss the resulting tradeoffs. These tradeoffs, as we show, are fundamental to the nature of the problem and are independent of either of the above-mentioned techniques.

### A. Minimum-Variance Beamforming

Consider a signal $\mathbf{s}(\theta)$ whose structure is parameterized by $\theta$ and measured in the presence of other signals and noise. By applying the correct weight vector $\mathbf{h}$ to the measurement vector $\mathbf{y}$, $\mathbf{s}(\theta)$ can be emphasized while noise and signals with different values of $\theta$ can be suppressed. The minimum variance criterion for specifying $\mathbf{h}$ is to minimize the average power, $\mathrm{E}[|\mathbf{h}^{\mathrm{H}}\mathbf{y}|^2]$, at the output of the filter subject to the constraint that the desired signal with parameter value $\theta$ is not suppressed. The desired signal constraint is mathematically specified by $\Re[\mathbf{s}^{\mathrm{H}}(\theta)\mathbf{h}] = 1$. Hence, the optimization problem is stated as

$$\min_{\mathbf{h}} \mathrm{E}[|\mathbf{h}^{\mathrm{H}}\mathbf{y}|^2] \qquad \text{subject to} \quad \Re[\mathbf{s}^{\mathrm{H}}(\theta)\mathbf{h}] = 1 \tag{3}$$

and the solution is given by

$$\mathbf{h} = \frac{\mathbf{R}_{\mathbf{y}}^{-1}\mathbf{s}(\theta)}{\mathbf{s}^{\mathrm{H}}(\theta)\mathbf{R}_{\mathbf{y}}^{-1}\mathbf{s}(\theta)} \tag{4}$$

where $\mathbf{R_y}$ is the covariance matrix of the measurements. As can be seen, the optimum weight

vector is a function of the covariance matrix $\mathbf{R}_{\mathbf{y}}$ and the assumed direction of propagation. Instead of calculating $\mathbf{h}$, however, we can directly compute the minimum-variance spectrum by calculating the power in the beamformer's output as a function of parameter $\theta$ according to

$$P(\theta) = [\mathbf{s}^{\mathrm{H}}(\theta)\mathbf{R}_{\mathbf{y}}^{-1}\mathbf{s}(\theta)]^{-1}. \tag{5}$$

In principle, the minimum-variance spectrum of (5) can be directly applied either in the element-space domain or the beamspace domain. If operating in the element domain, the signal vector $\mathbf{s}(\theta)$ is simply interpreted as the steering vector of phase shifts that are measured by a multi-channel array due to a signal arriving from direction $\theta$. Likewise, the $(m,n)$ element of the covariance matrix $\mathbf{R}_{\mathbf{y}}$ represents the correlation between measurements collected at the $m$th and the $n$th antenna elements. This element-domain covariance matrix can be estimated by averaging the outer product of the element-domain data vector over many data snapshots. If operating in the beamspace domain, then $\mathbf{s}(\theta) = \mathbf{a}(\theta)$ is the vector of measurements that a plane wave from direction $\theta$ excites at the output of the real-beam antenna as the beam is swept across the scene. The $(m,n)$ element of the covariance matrix $\mathbf{R}_{\mathbf{y}}$ in this case refers to the correlation between the output of the $m$th beam position and the $n$th beam position. This beamspace covariance matrix can be estimated by averaging the outer product of the data vector formed from the outputs of the different beam positions in an angular sweep. The averaging is performed over multiple sweeps. For either domain, the number of snapshots required to get a good estimate of $\mathbf{R}_{\mathbf{y}}$ is approximately twice the size of $\mathbf{R}_{\mathbf{y}}$. Note that this number can be reduced by employing diagonal loading, a simple yet effective method [13].

For noncoherent signals that fluctuate relative to each other from azimuth sweep to azimuth sweep, the above technique works very well with no modification and we will not discuss it further. For coherent targets, however, the minimum-variance technique will not work in either beamspace or element space. In order to break up this coherence, we wish to apply spatial smoothing in the element-space domain. First, the beamspace data snapshot is transformed to a virtual element-space snapshot by using a modified inverse discrete Fourier transform (mIDFT). The modified transform compensates for two factors. One factor has to do with the amplitude taper in the element-space domain resulting from the actual shape of the beamspace antenna pattern. The second factor is due to the real-beam positions being uniformly spaced in angle rather than spatial frequency. Uniform sampling in angle leads to nonuniform sampling in frequency because the relationship between spatial frequency $\Omega$ and the azimuth angle $\theta$ is nonlinear according to

$$\Omega = \frac{2\pi}{\lambda}\sin(\theta) \tag{6}$$

where $\lambda$ is the wavelength of the narrowband source. We briefly discuss both modifications in the following subsection.

## B. Modified IDFT

Consider the continuous inverse Fourier transform

$$\breve{y}(x) = \frac{1}{2\pi}\int_{-\infty}^{+\infty}\tilde{y}(j\Omega)e^{j\Omega x}d\Omega \tag{7}$$

where $\Omega$ is an analog frequency in radians per units of $x$. Suppose that $\tilde{y}(j\Omega)$ is the signal spectrum as observed through a finite antenna aperture. The smoothing of the observed signal spectrum caused by the specific pattern of the antenna corresponds to weighting the element-space data with a taper $t(x)$ that is the inverse Fourier transform of the antenna beampattern. For example, a uniform amplitude taper in the $x$-domain corresponds to a sinc-shaped beam in the $\Omega$ domain. Furthermore, the width of the taper $t(x)$ is inversely related to the width of the beam in the $\Omega$ domain. Since most antennas do not have a sinc-shaped beampattern, the corresponding taper $t(x)$ is not uniform and must be compensated for if we want the source power to be uniform in the element domain. Therefore, we express the element-domain snapshot data as $\breve{y}(x) = t(x)y(x)$, and the inverse Fourier transform becomes

$$\breve{y}(x) = t(x)y(x) = \frac{1}{2\pi}\int_{-\infty}^{+\infty}\tilde{y}(j\Omega)e^{j\Omega x}d\Omega. \tag{8}$$

As mentioned, the inverse transform in (8) gives the tapered data $\breve{y}(x)$. To obtain untapered data, we move $t(x)$ into the transform to obtain

$$y(x) = \frac{1}{2\pi}\int_{-\infty}^{+\infty}\frac{\tilde{y}(j\Omega)}{t(x)}e^{j\Omega x}d\Omega. \tag{9}$$

Since the beamspace data are collected at discrete beam positions, and we wish to obtain virtual element-space data which are also discrete, we need a discrete transform. Discretizing the data in both domains yields

$$y(n\Delta x) = \frac{1}{2\pi}\sum_{k=0}^{N_b-1}\frac{\tilde{y}(j\Omega_k)}{t(n\Delta x)}e^{j\Omega_k n\Delta x}\Delta\Omega_k, \qquad n = 0,1,\ldots,N_v-1 \tag{10}$$

where $N_v$ is the number of virtual array elements that we wish to obtain in the spatial-domain. It is important to note that the interpolated spatial sampling is uniform while frequency sampling is not, which is why we denote the discrete frequency bins as having width $\Delta\Omega_k$ rather than some uniform $\Delta\Omega$. The relationship between the uniform angular sampling $\Delta\theta$ and the nonuniform frequency sampling follows

directly from (6). Defining normalized discrete frequency to be $\omega_k = \Delta x \Omega_k$, we obtain the following mIDFT

$$y_n = \frac{1}{2\pi t_n} \sum_{k=0}^{N_a-1} \tilde{y}(j\omega_k) e^{j\omega_k} \Delta\omega_k, \qquad n = 0, \ldots, N_v - 1 \tag{11}$$

where $\tilde{y}(j\omega_k)$ is the beamspace measurement obtained at the $k$th beam position and $t_n$ is the amplitude taper at $t(n\Delta x)$. We can rewrite the transform (11) in matrix-vector form as

$$\mathbf{y} = \mathbf{W}\tilde{\mathbf{y}} \tag{12}$$

where $[W]_{nm} = (1/2\pi t_n) e^{jn\omega_m} \Delta\omega_m$. Thus, (12) transforms the nonuniformly sampled real-beam data to an untapered virtual array in element space.

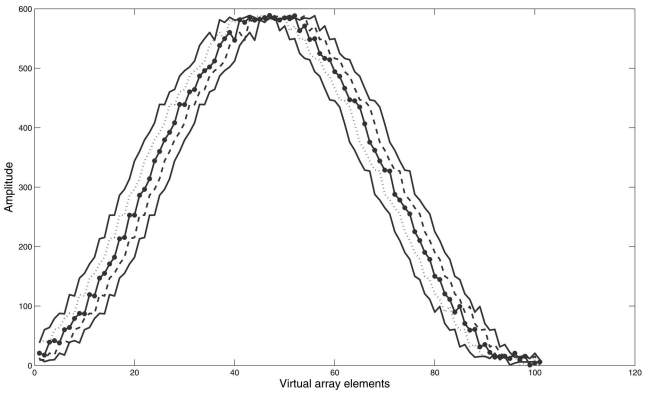


Fig. 3. Transformation of beamspace data to element-space data consisting of 100-element shifted virtual subarrays. The shift between any two virtual subarrays is $2B^{-1}$. The figure shows nonuniform SNR profile.

## C. Nonuniform SNR

We can express the beamspace snapshot vector in (2) as

$$\tilde{\mathbf{y}} = \tilde{\mathbf{y}}_s + \tilde{\mathbf{n}} \tag{13}$$

where $\tilde{\mathbf{y}}_s$ is the signal component and $\tilde{\mathbf{n}}$ is the receiver noise. Note that the signal part of the beamspace data $\tilde{\mathbf{y}}$ has been shaped by the beampattern of the real antenna. Thus, the transformation (12) is required to convert the beamspace data to the data that would have been received by an untapered multi-channel array, i.e., a virtual array. The beamspace noise contribution, however, does not follow the beampattern because it is due to internal receiver noise and not the result of a propagating signal received by the antenna.

Applying the mIDFT transform to the noisy beamspace data yields

$$\mathbf{W}\tilde{\mathbf{y}} = \mathbf{W}\tilde{\mathbf{y}}_s + \mathbf{W}\tilde{\mathbf{n}}. \tag{14}$$

Let us simplify this situation further, for the sake of explanation, by considering a scenario where $\tilde{\mathbf{y}}_s$ consists of only one source signal. The average power of this signal in each virtual array element is determined by the diagonal of $\mathrm{E}[\mathbf{W}\tilde{\mathbf{y}}_s\tilde{\mathbf{y}}_s^{\mathrm{H}}\mathbf{W}^{\mathrm{H}}]$. The taper term in the denominator of (11) normalizes the expected signal power to be uniform across all virtual elements. On the other hand, the noise covariance for the virtual array is

$$\mathrm{E}[\mathbf{W}\tilde{\mathbf{n}}\tilde{\mathbf{n}}^{\mathrm{H}}\mathbf{W}^{\mathrm{H}}] \approx N_{\mathrm{beam}}\sigma_n^2 \mathrm{diag}(t_0^{-2}, t_1^{-2}, \ldots, t_{N_v-1}^{-2}) \tag{15}$$

where diag$(\cdot)$ forms a diagonal matrix out of the elements of a vector and we have ignored the fact that the mIDFT transformation is not strictly an orthogonal transformation. The validity of this assumption depends on the angular span of the real-beam data. If the data amplitude taper $t(x)$ is nonuniform, then (15) shows that the noise power is not uniform across the virtual array. Unfortunately, if we correct for the nonuniform average noise power by multiplying by the amplitude taper, we will achieve uniform average noise power, but will cause nonuniform average signal power. We wish to maintain uniform signal power in the virtual element domain so that spatial smoothing can be used to break signal coherence. Hence, we are faced with nonuniform SNR on each array element. Although we are able to create multiple shifted virtual arrays with identical structure, the SNR-per-element of each virtual array will be different. This results in a fundamental problem where the covariance matrices corresponding to different virtual arrays are not equal. In addition, the eigenvalues of the noise subspace are no longer equal, which complicates the ability to separate signal and noise subspaces. However, when applying spatial smoothing to break signal coherence, it is more important to have uniform signal power across the array than it is to have uniform noise power across the array.

There are a couple of important points to consider here. First, the nonuniform SNR profile results from the shaping of the data by the antenna beampattern and is inherent to the data collection model. Second, our approach is different from Ly's method [8], which applies smoothing directly to the real-beam data. The difference is two-fold. 1) Beamspace smoothing results in a different signal profile in different angular spans as opposed to a nonuniform SNR profile. Thus the resulting covariance matrices have unequal signal components. 2) In our approach, even though we inherently have a nonuniform SNR profile, we explicitly attempt to ensure that the signal component is uniform across the array, as required by the spatial smoothing technique.

The mIDFT transformation can be performed several times to obtain data for several virtual arrays shifted by different amounts [7]. Fig. 3 shows five 100-element virtual arrays with the uncompensated amplitude taper. Specifically, if we look at the

amplitude for the same element index across the five virtual arrays, we see that they have different signal strengths. In typical applications of spatial smoothing, the subvectors of the data snapshot in element-space domain may have little or no overlap. This is not an option in our application as nonoverlapping virtual arrays would result in extremely disparate noise-power characteristics between subarrays. Thus, the choice of shift between virtual arrays embodies the fundamental tradeoff in this application. By selecting small shifts, the disparity in SNR characteristics of the shifted virtual arrays is minimized, but the ability to counteract signal coherence is degraded. On the other hand, virtual arrays with large shifts would have better smoothing effect on the signal coherence, but would cause corrupted covariance estimates due to varying noise characteristics.

To summarize, the data from each beamspace sweep is transformed to several shifted element-space snapshots using the mIDFT. The interpolated data for each shifted virtual array is treated as a subvector to obtain a final covariance estimate via the spatial smoothing algorithm. Once this final covariance estimate is obtained, the minimum-variance signal spectrum can be estimated, but performance will be degraded by nonuniform SNR characteristics across the different virtual arrays.

### D. Swath Subsectioning

We now exploit the fact that the beamspace data due to a single source is highly localized to an angular region where the antenna beam is approximately aligned with that source's DOA. This fact allows for a reduction in computational complexity as well as improved performance. In this method, we divide the full FOV covered by a sweep of the antenna beam into several subswaths, or subsections. We then apply root minimum-variance beamforming to estimate the DOAs of sources present within a given subsection. The advantage of using a root-based technique is that it gives better resolution than the minimum-variance spectrum for the same SNR [14]. Details on root minimum-variance beamforming are available in [10] and [14].

The swath subsectioning reduces computational complexity and increases the convergence rate of the covariance matrix estimates. Each swath subsection has a reduced angular extent; hence, it also has a smaller spatial bandwidth. Since the required element spacing $\delta d$ of the virtual array is inversely related to the spatial bandwidth of the arriving sources, reduced bandwidth implies that the spacing between virtual elements can be increased without violating Nyquist's sampling theorem. The ability to increase the spacing between virtual array elements allows the virtual array aperture length (and, hence, the same array resolution) to be represented with fewer elements. This reduces the size of the element-domain covariance matrix, which reduces the sample support required to obtain quality covariance estimates. Computational complexity is reduced because the required matrix inverses are now applied to smaller matrices, but more importantly, performance is improved by increased convergence of the covariance estimates.

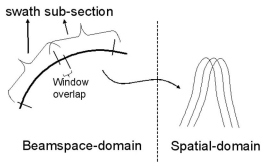


Fig. 4. Swath subsectioning by moving sliding window over beamspace. Partial overlap at edge of each subsection avoids discontinuities.

The swath subsectioning approach can be thought of as moving a sliding window over the beamspace data as illustrated in Fig. 4. Each window location filters the spatial spectrum of arriving sources. The filtered azimuth spectrum is then transformed to the element-space domain for several virtual arrays, spatial smoothing is applied, and finally the roots of the spectral polynomial are obtained. For a given subsection, the first $N_s$ roots lying closest to the unit circle in the complex plane are assumed to correspond to $N_s$ signal DOAs.

Computing roots to estimate signal DOAs using swath subsectioning requires two additional steps. The first involves overcoming the aliasing resulting from different angular (and as a result spatial frequency) ranges covered by swath subsections having a fixed bandwidth. The second step is the mapping of the estimated DOA from the swath subsection to the FOV. We discuss both steps in detail.

Consider a swath subsection spanning an angular range from $\phi_1$ to $\phi_2$ lying wholly within the full system FOV. From (6) we see that this angular range defines a spatial frequency range from $\Omega_1 = 2\pi \sin(\phi_1)/\lambda$ to $\Omega_2 = 2\pi \sin(\phi_2)/\lambda$ and hence a spatial bandwidth $B = \Omega_2 - \Omega_1$. The spatial bandwidth in turn defines the virtual array element spacing $\delta d = 2\pi/B$, which can be used to obtain the normalized spatial frequencies $\omega_1 = \Omega_1 \delta d$ and $\omega_2 = \Omega_2 \delta d$. Note that the virtual array spacing is based on the spatial bandwidth of the swath subsection, not of the full FOV. Also, since $\delta d$ has been chosen to satisfy Nyquist sampling for the subswath, we have $\omega_2 - \omega_1 = 2\pi$, and the normalized spatial bandwidth of the subswath corresponds to a single trip around the unit circle in the z-plane.

In general, however, $\omega_1 \neq -\pi$ and $\omega_2 \neq \pi$. Hence, the path around the z-plane unit circle for a given swath subsection does not generally have a mid-point located at zero. This asymmetry means that for polynomial-based DOA algorithms applied to the data from a subswath, a root on the positive real axis

does not necessarily correspond to a source arriving from the middle of the subswath. In other words, each subswath has a unique clockwise or counterclockwise rotation of its normalized spatial frequencies in the z-plane.

To correct this rotation, we simply need to know the normalized spatial frequency $\omega_1$ corresponding to the start of the subswath. If the swath subsection data leads to a polynomial root with angle $\omega_s$ that is deemed to correspond to a signal source, the nonnormalized spatial frequency $\Omega_s$ with respect to the full FOV is

$$\Omega_s = \Omega_1 + \frac{(\omega_s - \omega_1)}{\delta d}. \tag{16}$$

The estimated signal DOA can then be calculated by substituting $\Omega_s$ into (6).

The procedure above is applied to multiple swath subsections in order to cover the full FOV. However, there is the possibility of discontinuities in the beamspace data if a source DOA corresponds to the endpoints of a subswath. To avoid these discontinuities, we apply partially overlapped subsections. The midpoint of the overlapped region is used as a boundary in accepting any DOA estimates from a given subswath. By using overlapped subswaths, we insure that the sweep of the real-beam antenna pattern across the source DOA is fully contained within a subswath. In other words, the subswath endpoint does not occur until after the source has fallen out of the mainlobe and primary sidelobes of the real-beam sweep. This minimizes any truncation error that may occur due to the subsection approach. Alternatively, the reduced spatial bandwidth of the subswath means that larger virtual array spacing can be used. This larger spacing means that the virtual array can consist of fewer virtual elements, which reduces computational complexity and reduces the amount of data needed for obtaining a good estimate of the data covariance matrix needed for the minimum-variance beamformer.

In Fig. 5 we show three targets placed in the antenna beam's FOV spanning from $-15^\circ$ to $15^\circ$. Two of the targets are separated by less than an antenna beamwidth while the third target has a very different DOA. We use a subsection window size of $7.5^\circ$ to resolve these three targets based on the swath subsectioning method explained above. The figure illustrates the stitching together of different subswaths to produce the entire FOV including the superresolved signals.

## V. RESULTS

To analyze our proposed approach, we place two coherent sources separated by less than an antenna beamwidth. The sources have equal amplitude and phase, and are placed at $0.41^\circ$ and $0.59^\circ$. The 3 dB

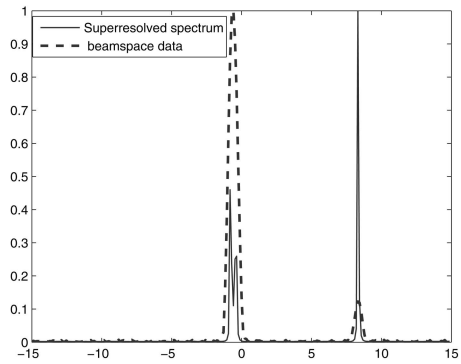


Fig. 5. Three signals resolved using swath subsectioning method with window length of $7.5^\circ$. Two of the signals are closely spaced and lie in same swath subsection while third one lies in entirely different swath subsection. This figure shows "stitching" together of different swath subsections to produce spectrum estimate of entire FOV ranging from $-15^\circ$ to $15^\circ$.

antenna beamwidth is $0.44^\circ$, which makes the sources about two-fifths of a beamwidth apart. The antenna beam covers an azimuth angular range from $-15^\circ$ to $15^\circ$.

Given the above setup, Figs. 6(a)–(d) show the the root mean-squared error (RMSE) metric versus SNR performance curves as a function of the virtual element array shift and subswath window size. The RMSE metric is defined as

$$\text{RMSE} = \sqrt{\text{E}\left[\sum_{i=1}^{Q}(\theta_i - \hat{\theta}_i)^2\right]} \tag{17}$$

where $\theta_i$ is the true DOA for the $i$th source and $\hat{\theta}_i$ is the estimated DOA for the same source. The total number of sources in this simulation is $Q = 2$. The expectation in (17) is estimated by averaging the algorithm performance over 500 Monte Carlo trials. For each subswath in a trial, we interpolate the data received by several virtual subarrays, each shift by a particular amount with respect to the previous subarray. For example, a shift of "0.5" indicates that all subarrays are shifted by $0.5\delta d$ with respect to each other. The virtual subarray data is used in the spatial smoothing algorithm to obtain a smoothed covariance matrix, which is then used in the root minimum-variance distortionless response algorithm.

From Fig. 6, we observe the following.

1) The error is less for small subswath window sizes, regardless of shift size.

2) For a specific window size, performance initally improves with increasing subarray shift, but then begins to degrade. A shift of one element seems to perform best.

3) There does seem to be a threshold SNR where performance begins to improve dramatically, and the threshold SNR seems to shift to lower SNR for smaller subswath window size. The threshold phenomenon is common in estimation problems [10].

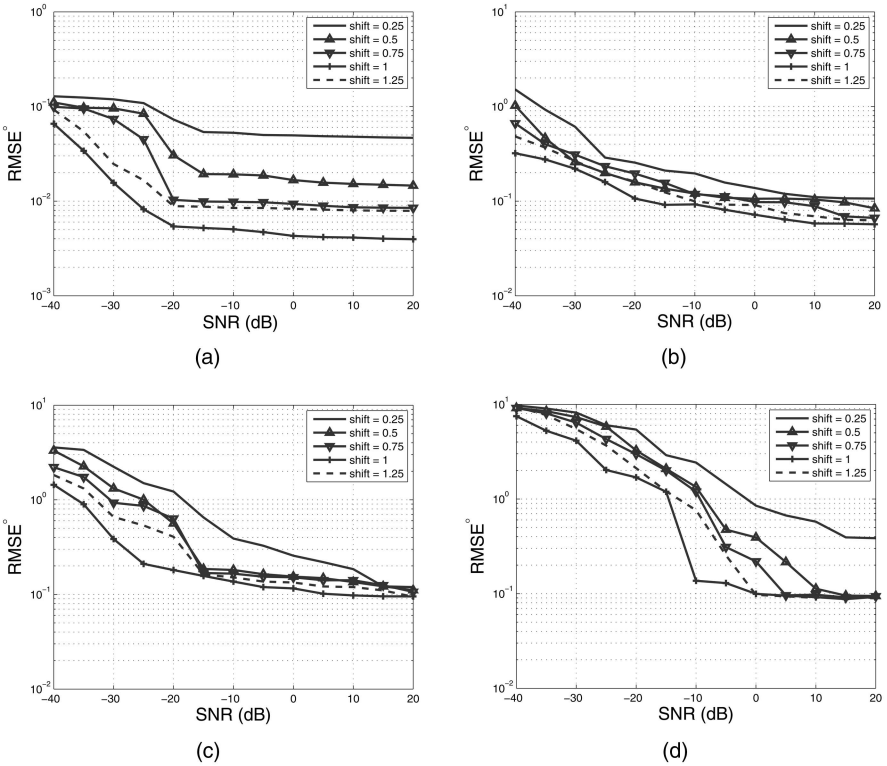


Fig. 6. RMSE versus SNR plots for different shifts and window lengths. Shift of 0.25 means that each virtual element array is shifted from previous one by one-fourth of virtual element spacing. (a) Window length = 3.25°. (b) Window length = 7.5°. (c) Window length = 15°. (d) Window length = 30°. Note that window length of 30° covers entire azimuth angular range.

For our approach, performance at low SNR improves with reduced window size.

The reason for improved performance with decreasing window size is likely due to improved convergence of the estimated covariance estimate. The number of data samples necessary to obtain a good estimate is proportional to the size of the matrix. Since the swath subsection approach increases virtual array element spacing, it reduces the number of virtual array elements necessary for a given array size. This reduces the dimensions of the data covariance matrix and improves the convergence of its estimate. Furthermore, the important data for estimating a given DOA are largely localized to a few real-beam positions where the antenna mainlobe is nearly aligned with the DOA. At other beam positions, the source's contribution to the measured data is small since the source must pass through low sidelobes. This means that error induced by truncating the beamspace data window is insignificant relative to the large performance improvement obtained through better convergence of covariance estimates.

The reason for the second observation follows from the fundamental tradeoff that exists between the nonuniformity of SNR profiles across the shifted virtual element arrays and the degree to which signal coherence is broken by those shifts. For small shifts, the effect of nonuniform SNR profile across the shifted arrays is small, but the ability of the shifted arrays to break the coherent signal structure is weak. For large shifts, signal coherence can be easily broken but the shifted virtual arrays have significantly disparate SNR profiles. A shift of one virtual array element seems to be a good compromise between these competing requirements.

We next compare the performance of MUSIC and minimum-variance beamforming. In Fig. 7 we plot the MUSIC and minimum-variance beamforming RMSE error in estimating $\theta_1$ in the presence of $\theta_2$. All results are for a virtual subarray shift of one virtual element. We note that, as expected, both MUSIC and minimum-variance beamforming follow similar trends, although the latter seems to perform better for small window size and at lower SNR. Plotting the RMSE for one DOA in the presence of the other also allows us to compare our results with the Cramer-Rao bound. Strictly speaking, the Cramer-Rao lower bound is a bound on the variance of an unbiased estimate of a nonrandom parameter, not for the RMSE metric that we use here. However, it helps us better analyze our results in the following discussion.

Fig. 7 shows that the RMSE performance of minimum-variance beamforming and MUSIC tends toward the Cramer-Rao bound for decreasing window size and lower SNR. Both methods, however, possess a pronounced performance floor. We analyze this further for window size of 30°, which has the worst performance. The separation of RMSE into bias

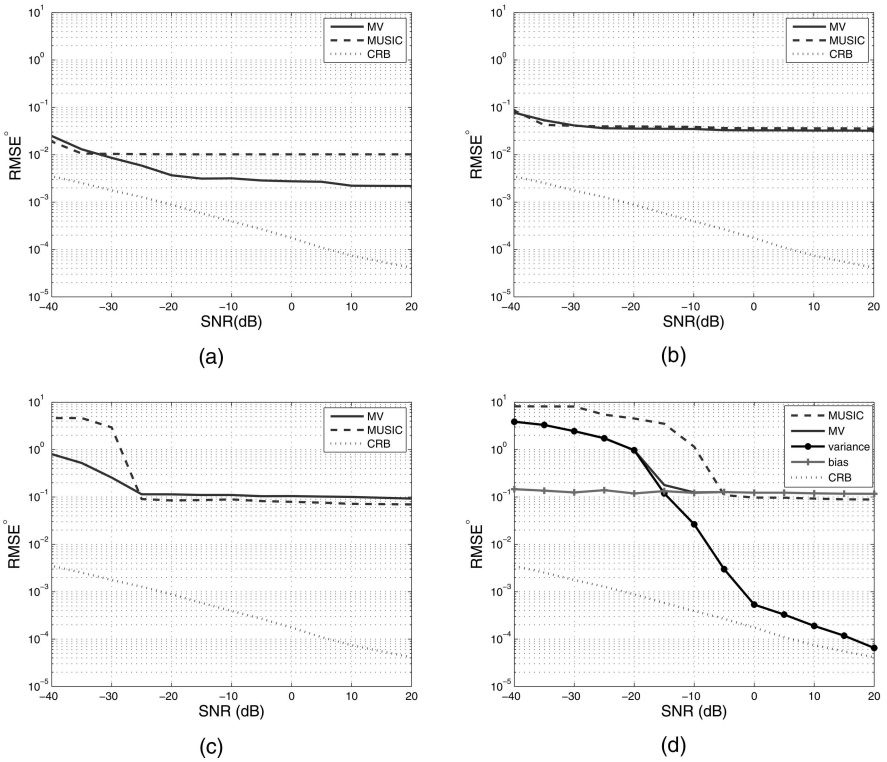


Fig. 7. RMSE for $\hat{\theta}_1$ versus SNR plots for different window lengths and shift of one virtual element. Shift of one element means that each virtual element array is shifted from previous one by one virtual element spacing. Minimum variance (MV) beamforming, MUSIC and Cramer-Rao bound plots are shown. (a) Window length = 3.25°. (b) Window length = 7.5°. (c) Window length = 15°. (d) Window length = 30°. Note that window length of 30° covers entire azimuth angular range. Fig. 7(d) also shows the bias and variance plots for MV beamforming.

and variance components for minimum-variance beamforming are plotted in Fig. 7(d). It can be seen that the performance floor for increasing SNR results from the presence of bias. The reason for this bias seems to be the fundamental nature of the data collection model which leads to nonuniform SNR profile across the virtual array. We are able to significantly improve performance by reducing the window size and exploiting the tradeoff between element array shifts and SNR disparity across these shifted arrays, but we cannot totally remove the bias.

## VI. CONCLUSION

In this paper we describe a fundamental problem that arises when resolving coherent targets separated by less than an antenna beamwidth when the data is collected in beamspace by sweeping a real antenna beam. We have explored the performance tradeoff between the nonuniform SNR profile that is observed over multiple shifted virtual arrays and the efficacy of spatial smoothing for different array shifts. We also proposed a swath subsectioning technique that reduces the number of virtual elements needed to populate a virtual array. This step improves performance by reducing computational complexity and reducing the amount of training data necessary to obtain quality covariance estimates. Our proposed method gives promising results for performing superresolution of coherent signals using real-beam data.

**SHIKHAR UTTAM**
**NATHAN A. GOODMAN**
**Dept. of Electrical and Computer Engineering**
**University of Arizona**
**1230 E. Speedway Blvd.**
**Tucson, AZ 85721**
**E-mail: (shikhar@ece.arizona.edu).**

REFERENCES

[1] Schmidt, R. O.
Multiple emitter location and signal parameter estimation.
*IEEE Transactions on Antennas and Propagation*, **34**, 3 (Mar. 1986), 276–280.

[2] Lee, H. and Wengrovitz, M.
Resolution threshold of beamspace music for two closely-spaced emitters.
*IEEE Transactions on Acoustics, Speech, and Signal Processing*, (Sept. 1990), 1545–1559.

[3] Rao, B. D. and Hari, K. V. S.
Performance analysis of root-music.
*IEEE Transactions on Acoustics, Speech, and Signal Processing*, **37** (Dec. 1989), 1939–1949.

[4] Zoltowski, M. D., Kautz, G. M., and Silverstein, S. D.
Beamspace root-music.
*IEEE Transactions on Signal Processing*, **41** (Jan. 1993), 344–364.

[5] Roy, R., Paulraj, A., and Kailath, T.
Esprit—A subspace rotation approach to estimation of parameters of cisoids in noise.
*IEEE Transactions on Acoustics, Speech, and Signal Processing*, **34** (Oct. 1986), 1340–1342.

[6] Shan, T. J., Wax, M., and Kailath, T.
On spatial smoothing for direction-of-arrival estimation of coherent signals.
*IEEE Transactions on Acoustics, Speech, and Signal Processing*, **33** (Apr. 1985), 806–811.

[7] Friedlander, B. and Weiss, A. J.
Direction finding using spatial smoothing with interpolated arrays.
*IEEE Transactions on Aerospace and Electronic System*, **28**, 2 (Apr. 1992), 574–587.

[8] Ly, C., Dropkin, H., and Manitius, A. Z.
An extension of the music algorithm to millimeter wave (MMW) real-beam radar scanning antennas.
*Proceedings of SPIE*, vol. 4744, Apr. 2002, 96–107.

[9] Johnson, D. and Dudgeon, D.
*Array Signal Processing: Concepts and Techniques*.
Upper Saddle River, NJ: Prentice-Hall, 1993.

[10] Trees, H. L. V.
*Optimum Array Processing*.
Hoboken, NJ: Wiley, 2002.

[11] Ziskind, I. and Wax, M.
Maximum likelihood localization of multiple sources by alternating protection.
*IEEE Transactions on Acoustics, Speech, and Signal Processing*, **36** (Oct. 1988), 1553–1560.

[12] Haykin, S., Litva, J., and Shepherd, T. J. (Eds.).
*Radar Array Processing*.
New York: Springer, 1993.

[13] Guerci, J.
*Space-Time Adaptive Processing for Radar*.
Norwood, MA: Artech House, 2003.

[14] Barabell, A.
Improving the resolution performance of eigenstructure-based direction-finding algorithms.
In *Proceedings of the IEEE International Conference on Acoustics, Speech, and Signal Processing* (ICASSP '83), vol. 8, Apr. 1983, 336–339.

## Comments and Further Results on "Observability of an Integrated GPS/INS During Maneuvers"

The above-mentioned paper [1] presented an observability analysis of GPS/INS during maneuvers based on a perturbation model. This note is on several issues regarding two theorems (Theorem 4 and Theorem 5) for the time-varying cases in [1], [2]. Specifically, this note points out and corrects several errors in the proof of Theorem 4, and extends Theorem 5 to yield full observability.

Firstly, it refers to the development below (18) in Theorem 4. As for the equation

$$\omega_{ie} \times X = b_5\mathbf{F} + b_6\dot{\mathbf{F}}, \qquad b_5, b_6 \in \Re \tag{1}$$

the authors stated that "If $b_5$ and/or $b_6$ are non-zero, then $\omega_{ie}$ should be perpendicular to the plane-$\mathbf{F}\dot{\mathbf{F}}$…." In fact, (1) only implies that $\omega_{ie}$ is perpendicular to the vector $b_5\mathbf{F} + b_6\dot{\mathbf{F}}$, not the entire plane-$\mathbf{F}\dot{\mathbf{F}}$. Note that there always exists, in any plane (including the plane-$\mathbf{F}\dot{\mathbf{F}}$), a vector to which $\omega_{ie}$ is perpendicular. Consequently, the conclusion $\omega_{ie} \times X = 0$ cannot be arrived at in this case. In addition, with Assumption 4 satisfied, $\omega_{ie} \times X = 0$ does not lead to $X = 0$.

In order to make Theorem 4 valid, Assumption 5 might be instead stated as "$\omega_{ie}$ lies in the plane-$\mathbf{F}\dot{\mathbf{F}}$." Then $\omega_{ie} \times X = 0$ is a direct result with (1) because $X$ is also in the plane-$\mathbf{F}\dot{\mathbf{F}}$ from [1, eq. (17a)]. Suppose $X = b_7\omega_{ie}$, $b_7 \in \Re$. Substituting into (16b) and (16a) in turns yields $0 = b_7\mathbf{F} \times \omega_{ie}$. It means $b_7 = 0$ with Assumption 4, so $X = 0$. Note that the revised Assumption 5 is physically a rare event. It is wondered whether a looser assumption exists.

Secondly, a couple of minor typing errors exist in Theorem 5 ([1, pp. 531–532]). Specifically, $v_2$ below (25) should be

$$v_2 = \begin{bmatrix} F^b - [\omega_{eb}^b]^\times \Theta^{-1}([\omega_{eb}^b]^\times - [\omega_{ie}^b]^\times)F^b \\ \Theta^{-1}([\omega_{eb}^b]^\times - [\omega_{ie}^b]^\times)F^b \end{bmatrix}. \tag{2}$$

Consequently, $\Phi_{b2}$ defined in Assumption 3 of Theorem 5 should be

$$\Phi_{b2} = \{\bar{O}_{4,3} + (\bar{O}_{4,4} - \bar{O}_{4,3}[\omega_{eb}^b]^\times)\Theta^{-1}([\omega_{eb}^b]^\times - [\omega_{ie}^b]^\times)\}. \tag{3}$$

Furthermore, Theorem 5 can be refined to obtain full observability.

Manuscript received September 1, 2008; revised March 8, 2009; released for publication July 29, 2009.

IEEE Log No. T-AES/46/3/937993.

Refereeing of this contribution was handled by D. Gebre-Egziabher.

This work was supported in part by the National Natural Science Foundation of China (60604011).